ELSEVIER

Reviews in Molecular Biotechnology 74 (2000) 207–231

REVIEWS IN Molecular Biotechnology

www.elsevier.com/locate/rmb

X-ray and neutron surface scattering for studying lipid/polymer assemblies at the air–liquid and solid–liquid interfaces

Jaroslaw Majewski[a,*], Tonya L. Kuhl[b], Joyce Y. Wong[c], Gregory S. Smith[a,1]

[a] *Manuel Lujan Jr. Neutron Scattering Center, LANSCE-12, MS H805, Los Alamos National Laboratory, Los Alamos, New Mexico 87545, USA*

[b] *Materials Research Laboratory, University of California, Santa Barbara, CA 93106, USA*

[c] *Department of Biomedical Engineering, Boston University, 44 Cummington Street, Boston, MA 02215, USA*

Abstract

Simple mono- and bilayers, built of amphiphilic molecules and prepared at air–liquid or solid–liquid interfaces, can be used as models to study such effects as water penetration, hydrocarbon chain packing, and structural changes due to head group modification. In the paper, we will discuss neutron and X-ray reflectometry and grazing incidence X-ray diffraction techniques used to explore structures of such ultra-thin organic films in different environments. We will illustrate the use of these methods to characterize the morphologies of the following systems: (i) polyethylene glycol-modified distearoylphosphatidylethanolamine monolayers at air–liquid and solid–liquid interfaces; and (ii) assemblies of branched polyethyleneimine polymer and dimyristoylphophatidylcholine lipid at solid–liquid interfaces.

Keywords: Grazing incidence X-ray diffraction; Neutron and X-ray reflectivity; Lipid membranes; Polymers; Air–liquid interface; Solid–liquid interface

1. Introduction

In recent years, several scattering techniques have been developed for probing the surface structure of materials. These include neutron and X-ray reflectometry and X-ray grazing incidence diffraction (GID) (Eisenberger and Marra, 1981; Als Nielsen and Kjaer, 1989; Feidenhans'l, 1989; Russell, 1990; Als-Nielsen et al., 1994). In each of these surface-sensitive scattering methods, one takes advantage of the wave properties of the

* Corresponding author. Fax: +1-505-665-2676.

E-mail addresses: jarek@lanl.gov (J. Majewski), gsmith@lanl.gov (G.S. Smith).

[1] Co-corresponding author.

1389-0352/00/$ - see front matter © 2000 Published by Elsevier Science B.V.
PII: S1389-0352(00)00011-8

probe (electromagnetic radiation or the neutron) near the condition of perfect reflection from the sample. As shown by the latest reports (Russell, 1990; Als-Nielsen et al., 1994), these techniques can be successfully implemented for studying structures of organic, ultra-thin, layered molecular arrays at various interfaces with Å resolution.

Structural studies of bulk, layered, polycrystalline molecular assemblies provide information about characteristic repeat distances, molecular conformations, chain packing properties, magnitude of the molecular motion or surface roughness of the layers, hydration and inter-layer arrangements (Janiak et al., 1976, 1979). It is not clear, however, how many of the bulk properties are preserved in single monolayers and bilayers. In the case of these ultra-thin organic structures, standard diffraction techniques are not applicable because of the low, scattered signal rates and substantial background contribution. Therefore, the task of the surface sensitive scattering methods is to maximize the signal or to reduce the thermal diffuse scattering from the bulk to a level where surface signal can be observed with reasonable statistics.

2. Reflectometry

The reflectivity of a surface is defined as the ratio of the number of particles (neutrons or photons) elastically and specularly scattered from the surface to the number of incident particles. When measured as a function of wavevector transfer (defined below), the reflectivity curve contains information regarding the sample-normal profile of the in-plane average of the coherent scattering cross-sections. X-rays are scattered from the electrons, whereas, neutrons are scattered from nuclei. As will be shown below, the X-ray (neutron) reflectivity yields a profile of the electron density (coherent neutron scattering length density, SLD). If one knows the chemical constituents of the investigated system and the electron density or SLD distribution, the concentration of a given atomic species at a particular depth can then be calculated.

2.1. Neutron reflectometry

Detailed theoretical descriptions of the X-ray and neutron reflectometry have been given in literature (Als-Nielsen, 1986a; Russell, 1990; Smith and Majkrzak, 1999). To summarize basic principles of the technique lets consider the situation shown in Fig. 1 where a neutron is incident on a flat substrate covered with a thin layer of a material. That neutron may be reflected, transmitted or refracted. In addition, each of the de-Broglie waves associated with the moving neutron may interfere constructively or destructively with the other. To understand how these measure-

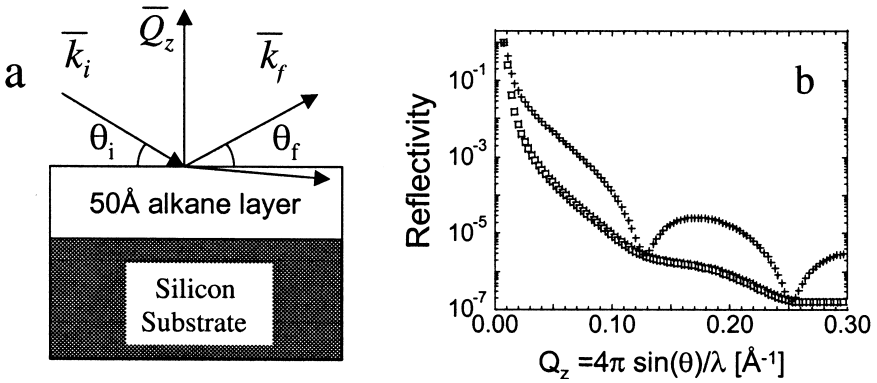

Fig. 1. (a) Schematic of a reflection experiment with a hydrocarbon layer on a silicon substrate (for specular reflection $\theta_i = \theta_f$) and (b) calculated reflectivity curve for system shown in Fig. 1a. The upper curve is calculated for a deuterated layer and the lower curve is for a protonated alkane layer.

ments yield information regarding the flat material, we begin by considering that far from the source, the incident neutron can be treated as a plane wave with wavevector, $\vec{k}_i$. The magnitude of the wavevector in air is given by:

$$|\vec{k}_i| = k_i = \frac{2\pi}{\lambda} = \frac{m_n v_i}{\hbar} \quad (1)$$

where λ is the neutron wavelength, v_i is the velocity of the neutron, $\hbar$ is Planck's constant divided by 2π, and m_n is the mass of the neutron. $|\vec{k}_f| = |\vec{k}_i| = k_0$ for elastically scattered neutrons. We then look for wave functions that satisfy the one-dimensional Schrödinger wave equation (since the component of the neutron $\vec{k}_i$ vector parallel to the surface is conserved during the scattering process). In air, the wave function at the interface between the layer and the air is described by:

$$\psi(z) = e^{ik_i z} + re^{-ik_i z} \quad (2)$$

Similarly, wave functions in the layer and the substrate can be written as

$$\psi(z) = Ae^{ik_{\text{layer}} z} + Be^{-ik_{\text{layer}} z} \quad (3)$$

$$\psi(z) = te^{ik_{\text{substrate}} z}, \quad (4)$$

respectively. In Eqs. (2)–(4), the k_i, k_{layer} and $k_{\text{substrate}}$ describe the components of the neutron wave vector normal to the interface.

The amplitude of the incoming wave is unity, of the reflected wave is r, and of the transmitted wave in the substrate is t. When one examines the current density of neutrons at the interface and if we define the reflectivity, R, to be the ratio of reflected neutrons to the number of incoming neutrons, we find that the reflectivity is simply the square of the amplitude of the reflected wave, $R = |r|^2$.

For specular reflection, the momentum transferred to the neutron in the collision is perpendicular to the surface and is given by:

$$Q_z = |\vec{k}_f - \vec{k}_i| = \frac{4\pi \sin(\theta_i)}{\lambda} \quad (5)$$

The energy of the neutron in free space is given by: $E = \hbar^2 k^2 / 2m_n$. Whenever the neutron encounters a material in space, that material presents a potential energy step to the neutron given by the Fermi pseudopotential:

$$V_{\text{Fermi}} = \frac{\hbar^2 k_c^2}{2m_n} \quad (6)$$

where k_c is related to the number of nuclei per unit volume of type i (i.e. the density of atoms of a particular chemical species) in the layer, N_i, and the coherent neutron scattering length of the nuclei of type i, b_i, by:

$$k_c^2 = 4\pi \sum_i N_i b_i = 4\pi\beta \quad (7)$$

where β is called the scattering length density (SLD). b_i may be complex with its imaginary component giving rise to absorption and the real part may be either positive or negative depending on the isotope (see for example the table in Lovesey, 1986). Conservation of energy dictates that:

$$k_{\text{layer}} = \sqrt{(k_0^2 - 4\pi\beta)} = \frac{m_n v_{\text{layer}}}{\hbar} \quad (8)$$

By matching wave functions and their derivatives at the interfaces (e.g. air-layer and layer-substrate), one can solve for R (Russell, 1990; Smith and Majkrzak, 1999), thus, the SLDs and thicknesses of the layers determine the reflectivity. Fig. 1b shows calculated reflectivity curves corresponding to the simple experiment in Fig. 1a. The goal of the reflectivity experiment is to measure $R(Q_z)$ and then infer $\beta(z)$ by fitting a model for the SLD to the data.

The example in Fig. 1a also highlights one of the advantages of neutron scattering. If we substitute deuterium for hydrogen, we would have a significantly different SLD (7.74×10^{-6} Å^{-2} vs. -0.41×10^{-6} Å^{-2} for deuterated and protonated hydrocarbon chains, respectively). This illustrates that by employing isotopic substitution, one can change the contrast between various parts of the system to gain a better understanding of their structures.

Fig. 1b also illustrates some of the common features found in reflectivity curves. Whenever the energy of the neutron is at or below the potential of the substrate (i.e. whenever $k_0^2 \leq 4\pi\beta_{\text{substrate}}$), the neutrons are perfectly reflected from the surface. The onset of total reflection is called the critical edge and the value of Q_z at that point is referred to as Q_{critical}. Also, Fig. 1b shows that fringes arise from interference between waves being reflected from the top surface and the buried interface between the substrate and the layer. For this simple case, the fringes have a spacing, $d_{\text{fringe}} = \dfrac{2\pi}{t_{\text{layer}}}$. The amplitude of the fringes relates to the contrast between the layers and the overall falloff of the curve obeys Fresnel law ($R \sim Q_z^{-4}$, Als-Nielsen, 1984). Finally, most interfaces are not discontinuous but are graded due to mixing or surface roughness. The surface roughness (characterized by the root mean square displacement from the average interface, σ) can also be obtained from the reflectivity curve (Nevot and Croce, 1980; Als-Nielsen, 1986b).

2.2. X-ray reflectometry

Essentially all of the discussion above describing neutron reflectometry is applicable to X-ray reflectometry. The basic difference is that neutrons are scattering from the nuclei where X-rays scatter from the charges in the system, the electrons (Braslau et al., 1985, 1988). In this case, we use the charge density instead of the scattering length density such that:

$$\beta(z) = r_0\rho_{el} - i\frac{\mu}{2\lambda} \tag{9}$$

where r_0 is the classical radius of the electron (2.82×10^{-5} Å), ρ_{el} is the electron density, μ is the X-ray linear absorption coefficient (averaged over the constituent atoms) and λ is the X-ray wavelength. As in the case for the neutrons, the imaginary term accounts for the absorption of the X-rays by the material.

2.3. Comparison of X-ray and neutron reflectometry

The ability to change contrast through isotopic substitution makes neutron reflection a powerful tool. However, neutron sources are inherently weak compared to the brilliance of available synchrotron light sources. This usually limits neutron reflectivity to a value of $R \sim 10^{-6}$ although lower values are possible to achieve by controlling the incoherent scattering background (Koenig et al., 1996). On the other hand X-ray reflectivities from liquid air interfaces down to $R \sim 10^{-10}$ are typical and allow one to probe larger values of Q_z (i.e. shorter length scales).

A big advantage of neutron scattering is the low absorption of neutrons in many solid state materials (for example, monocystalline silicon or quartz). This allows neutrons to penetrate through thick layers of substrate to probe buried, solid–liquid interfaces. Neutrons are virtually non-destructive for hydrocarbon layers but high flux synchrotron X-ray beams can damage organic films.

3. Grazing incidence diffraction (GID)

Due to low flux neutron sources, GID is generally used with intense synchrotron X-ray beams. The theory of grazing incident diffraction was first worked out by Vineyard (1982) and later applied to liquid surfaces (Als-Nielsen et al., 1982; Als-Nielsen, 1984; Als-Nielsen et al., 1994; Kjaer et al., 1987; Majewski et al., 1995). As discussed above, when the angle of incidence is below the critical angle, X-rays are perfectly reflected from the sample. In that case, the transmitted wave has a wave vector which lies in the plane of the surface. This, so called evanescent wave, does not travel deeply into the substrate, but instead decays exponentially as: $\psi(z) = e^{ik_{\text{substrate}}z}$, since $k_{\text{substrate}}$ is now a purely imaginary number. Adjusting the value of $k_{\text{substrate}}$ by changing the wavelength or angle, the penetration depth can be set to probe only the upper most surface (e.g. the top layer) (Als-Nielsen, 1986a). The wave

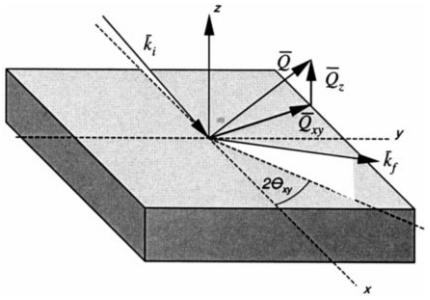

Fig. 2. Scattering geometry for GID.

travelling along the surface can be diffracted by the in-plane structure of the molecules at the surface. This scattering geometry is illustrated in Fig. 2.

By fixing $\vec{k}_i$ and adjusting the direction of $\vec{k}_f$, one can probe various values of $\vec{Q}$ since $\vec{Q} = \vec{k}_f - \vec{k}_i$. The scattered intensity is proportional to the structure factor, $S(\vec{Q})$:

$$S(\vec{Q}) \propto |f(\vec{Q})|^2 \times \left(GSF(\vec{Q})\right)^2 \quad (10)$$

where $f(\vec{Q})$ is the form factor of the molecule and $GSF(\vec{Q})$ is the geometrical structure factor. The GSF is the Fourier transform of the arrangement of the molecules. For two-dimensional systems, the GSF will not yield points in reciprocal space, but instead a series of *Bragg rods* (Kjaer, 1994). The form factor is the Fourier transform of the electron density of the molecule. For lipids in liquid crystalline phases their hydrocarbon chains are in an all *trans* configuration and freely rotating. In that case we can model them as cylinders of charge.

In general, Langmuir monolayers are composed of two-dimensional crystallites which are azimuthally randomly oriented on the water surface (i.e. two-dimensional powders). As stated above, the GID patterns from the two-dimensional ordered monolayers on the liquid surface arise from an array of *Bragg rods*, which extend parallel to the vertical scattering vector Q_z (Smith et al., 1988, 1990; Als-Nielsen and Kjaer, 1989; Kjaer, 1994). The scattered intensity is measured by scanning over a range of the horizontal scattering vector, $Q_{xy} = 4\pi \sin\theta_{xy}/\lambda$ (Fig. 2), where $2\theta_{xy}$ is the angle between the incident and diffracted beam projected onto the horizontal plane, and λ is the wavelength of the X-ray beam. Such a scan, integrated over the whole window of a linear position sensitive detector (PSD), which is placed parallel to the normal substrates, yields *Bragg peaks*. Simultaneously, the scattered intensity recorded in channels along the PSD, but integrated over the scattering vector in the horizontal plane across a Bragg peak, produces Q_z-resolved scans called *Bragg rod* profiles. Thus, GID provides data on the two-dimensional ordered portion of the monolayer. Several different types of information can be extracted from the measured Bragg peaks and Bragg rod profiles. The Q_{xy} positions of the Bragg peaks yield the repeat distances $d = 2\pi/Q_{xy}$ for the two-dimensional lattice structure. The resolution corrected full width at half maximum of the Bragg peak in Q_{xy} units yields the two-dimensional crystalline coherence length L, obtained by shape analysis of the Bragg peak through the Scherrer formula (Gunier, 1968). For the linear lipid tails, the square of the molecular form factor $|f(Q)|^2$ [Eq. (10)] is a disc-shaped function which reaches its maximum when the scattering vector $Q = (Q_{hk}, Q_z)$, where *h,k* are the Miller indices of a particular *Bragg rod*, is orthogonal to the molecular axis. Thus, when the molecules are vertical or tilted in a plane perpendicular to Q_{hk}, the maximum intensity along the Bragg rod will occur approximately at the horizon, for $Q_z \approx 0$ Å^{-1}. For molecules tilted otherwise, the Bragg rod maximum appears at a finite Q_z, dependent upon both the magnitude and direction of the tilt relative to the in-plane scattering vector Q_{hk}. Therefore, analysis of the intensity distribution along a Bragg rod provides information on the direction and magnitude of the molecular tilt, the length of the part of the molecule which scatters coherently, L_c, and the extent of molecular motion or surface roughness of the crystallites.

4. Polymer-modified lipid monolayers

Biological cells and extracellular matrices contain a variety of macromolecular structures sepa-

rated by an aqueous phase. One simple model for biological membranes is a lipid monolayer at the air–water interface. Several X-ray specular reflection and grazing incidence diffraction measurements have been performed on these systems (Helm et al., 1987a,b, 1991; Kjaer et al., 1987; Vaknin et al., 1991).

One way to increase the applicability of a lipid monolayer, to model a membrane with an extracellular matrix, is to incorporate lipids which expose hydrophilic polymers to the aqueous phase. These the so called polymer-lipids, have received much recent attention due to their application in drug delivery and biologically passivating coatings (Lasic and Martin, 1995; Sheth and Leckband, 1997; Halperin, 1998; Harder et al., 1998; Pertsin et al., 1998; Tirosh et al., 1998). The structure and surface properties of lipid assemblies before and after modification by the incorporation of polymer-lipids with their bulky, hydrophilic headgroups are of considerable importance for predicting monolayer, bilayer and liposome stability in such applications (Kenworthy et al., 1995a,b; Joannic et al., 1997; Szleifer et al., 1996).

4.1. X-ray grazing-incidence diffraction of polymer–lipid monolayers at the air–water interface

Polymer–lipids consisting of distearoylphosphatidylethanolamine (DSPE) with polyethylene glycol (PEG or EO_n of varying n) chemically grafted to the terminal amine of the headgroup were studied. These polymer-modified lipids serve as good models for terminally grafted polymers of low MW, where the 'grafting' density of the polymer chains can be varied and quantitatively controlled by simply varying the ratio of unmodified to polymer–modified lipid within a mixed monolayer or bilayer (Kuhl et al., 1994).

The X-ray reflection and GID experiments were performed on two systems (Majewski et al., 1998a; Kuhl et al., 1999):

- mixed, two-component, lipid monolayers composed of DSPE matrixed with 0, 1.3 or 9.0% of the same lipid with the PEG (2000 MW, 45 EO units) covalently linked to its headgroup, thereby forming DSPE–PEG_{2000}.
- mono-component DSPE-PEG monolayers, where the PE headgroup was systematically modified by chemically grafting smaller hydrophilic PEG chains of 90 MW (2 EO units), 350 MW (8 EO units), and 750 MW (17 EO units) to the lipid headgroup.

The monolayers were studied in a Langmuir trough (Fig. 3), at a surface pressure of 42 mN/m and 21°C. At these lipid packing densities, the PEG chains are submerged in the water subphase. The surface pressure was controlled by a barrier and measured with a tensiometer (Langmuir, 1917).

For di-acyl phospholipid monolayers at the air–water interface, diffraction is only observed from the lateral order of the tails; the headgroups are not ordered (Kjaer et al., 1987). Three hexagonal in-plane reflections: {1,0}, {1,1} and {2,0} (Fig. 4) are observable from the GID data for pure DSPE and mixed DSPE/DSPE–PEG monolayers ({hk} denotes a set of Bragg rods (hk) with equal in-plane components Q_{xy}, hence not resolved in GID from these two-dimensional powders; e.g. for hexagonal lattice {10} means $\{(10),(01),(\bar{1}0),(0\bar{1})(1\bar{1})(\bar{1}1)\}$)). All three compositions studied, 0, 1.3, and 9.0% DSPE–PEG have the same hexagonal unit cell dimension of $a_H =$ 4.70 Å, and thus the same repeat distance of $d_{10} = 4.07$ Å and a constant area per lipid molecule of 38.3 $Å^2$. However, the width of the Bragg peaks in Fig. 4 increase with DSPE-PEG concentration indicating that the size of two-dimensional crystallites decrease as more and more polymer–lipid molecules are introduced. It was found that the in-plane crystallite size is 360 Å for pure DSPE and decreases to 280 Å (230 Å) for 1.3% (9%) DSPE-PEG concentration. Fig. 5 shows the Bragg rods of the {1,0} reflections. The width of the Bragg rods increases systematically with increasing DSPE-PEG concentration. This means that the length, L_c, *normal* to the water surface, of Bragg scattering moieties of the lipid tails, gets shorter. One possibility could be that the molecules tilt more and more, thereby obtaining a shorter projection onto the surface normal.

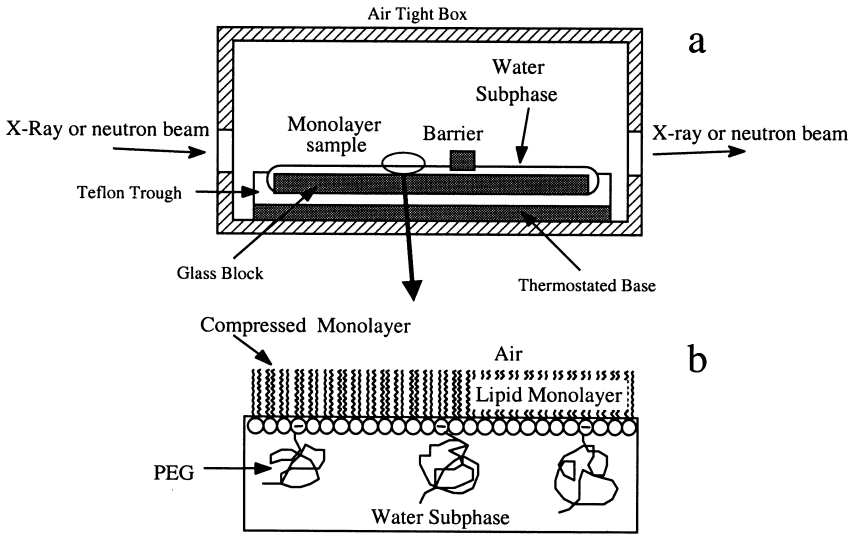

Fig. 3. (a) Schematic of a Langmuir trough; and (b) microscopic representation of a lipid film.

However, fitting a simple model of cylindrically symmetric and longitudinally uniform lipid tails (Als-Nielsen, 1994), a constant tilt angle of $t = 4° \pm 0.5°$ was found for all three concentrations. The observed increase in the width of the Bragg rods is therefore due to shorter and shorter portions of the molecules being in positional registry. A plausible model for this effect is depicted in Fig. 6. With increasing DSPE-PEG concentration the vertical position of the molecules becomes less and less ordered, and the tail end, as well as the tail part nearest to the head, therefore get space for lateral disorder and do not Bragg scatter. This model is in keeping with

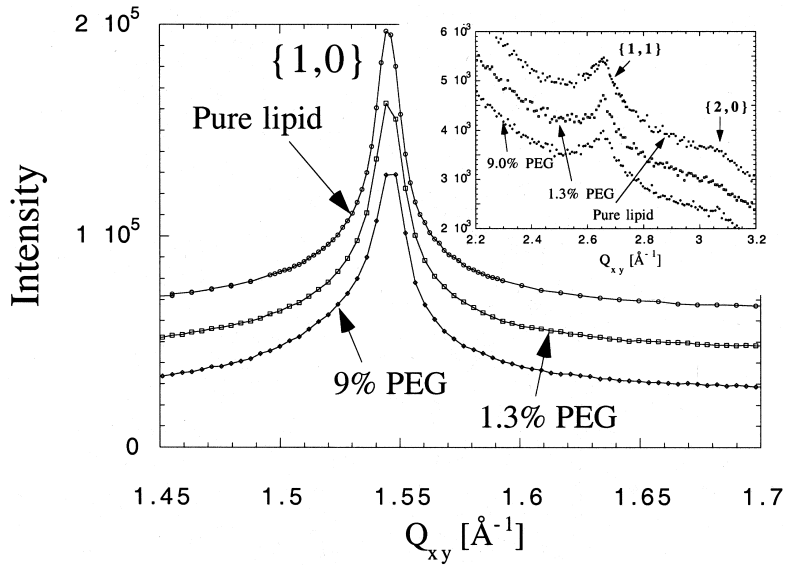

Fig. 4. The GID Q_z-integrated diffraction peaks of pure DSPE lipid and DSPE/DSPE-PEG$_{2000}$ mixed monolayers. For clarity {1,0} reflections were displaced by 4000 and the high order {1,1} and {2,0} reflection (shown in the inset) by 500 counts, respectively.

the chemical nature of the DSPE-PEG lipids. Compared to pure unmodified DSPE, the DSPE-PEG lipids have a bulky, hydrophilic headgroup composed of PE terminated by a 2000 MW methoxy-PEG chain. Because PEG is a water-soluble polymer, the DSPE-PEG lipids have a greater solubility than unmodified DSPE, as evidenced by a critical micellar concentration of 6×10^{-6} M compared to 1×10^{-12} M (Majewski et al., 1997). The increased solubility would result in a higher density of protrusions from the monolayer interface into the water subphase. The increase in size of the DSPE-PEG lipids might be expected to increase the lateral spacing of the lipids in the monolayer, but as shown above this does not take place: the dimension of the unit cell is unaffected by the DSPE-PEG concentration. A quantitative analysis of the width of the Bragg rods reveal that the length of the coherently diffracting lipid tails decreases from 23 Å for pure DSPE to 20 and 18 Å for 1.3 and 9.0% DSPE-PEG, respectively, consistent with the model discussed above.

The effect of disruption by PEG polymer is even more visible for mono-component monolayers built of DSPE with attached shorter hydrophilic polymer chains of 90 MW (2 EO, units), 350 MW (8 EO units), and 750 MW (17 EO units). The pressure–area isotherms for the four different DSPE-PEG_{MW} lipids are shown in Fig. 7. As can be seen, the PEG portion of the lipid headgroup is also surface active, and a non-zero surface pressure is detected even at very large areas per molecule. However, as the molecules are compressed, the DSPE-PEG_{MW} isotherms become almost superimposed, approaching that

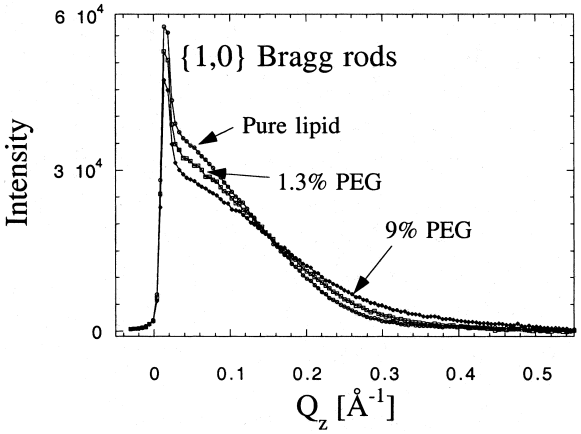

Fig. 5. The Bragg rod intensity profiles of the {1,0} reflection of pure DSPE lipid and DSPE/DSPE-PEG_{2000} monolayers. The sharp peak at $Q_z = 0.01$ Å^{-1} (Vineyard–Yoneda peak), arises from interference between X-rays diffracted up into the Bragg rod and rays diffracted down and then reflected back up by the interface. Solid lines are fits.

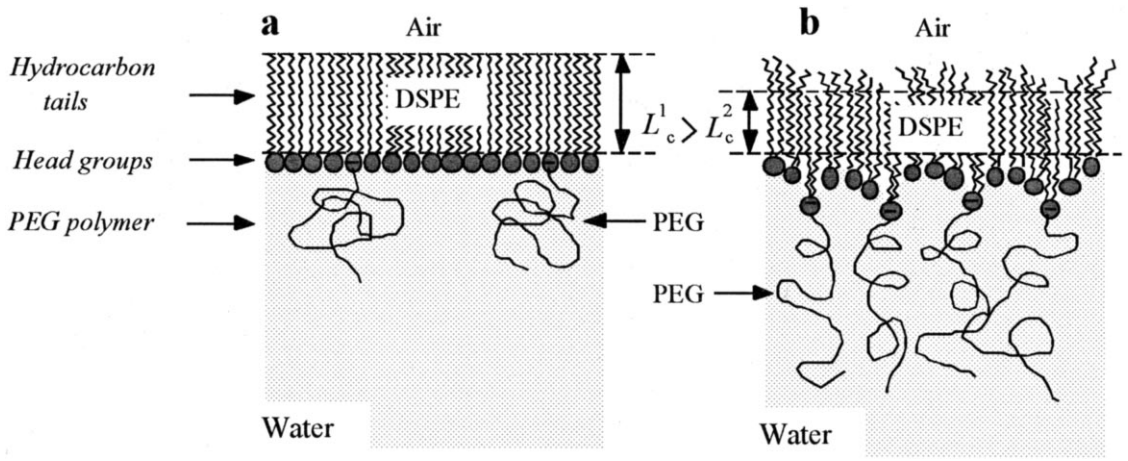

Fig. 6. Schematic structure of a mixed DSPE/DSPE–PEG_{2000} monolayer showing the decrease in length of the coherently scattering lipid tails due to the greater out of plane protrusions of the DSPE-PEG molecules from the two-dimensional plane of the monolayer, where L_c is the coherently scattering length. (a) For small percentages of PEG–lipid incorporated in to the monolayer, the polymers are non-interacting. (b) At higher concentrations, the PEG polymer headgroups stretch into solution, roughen the film surface, and reduce the out-of-plane thickness, L_c, of the ordered chains.

of unmodified DSPE, indicating that the PEG portion of the molecules is pushed down into the water subphase.

As shown in Fig. 4, for pure DSPE and mixed DSPE/DSPE-PEG_{2000} monolayers the {1,0} reflection and higher order hexagonal reflections {1,1} and {2,0} were observed. By contrast, only the {1,0} reflection was observable for the DSPE-PEG_{MW} monolayers. Fig. 8 shows the data projected on the Q_{xy}-axis, yielding Bragg peaks and intensities integrated over the Bragg peaks, as function of Q_z (the Bragg rods) are shown in Fig. 9. Clearly, for unmodified DSPE the peak is not split, indicating a hexagonal lattice of the chains. The Bragg rod exhibits one broad maximum, located at $Q_z \sim 0$ (Fig. 9). This indicates that the chains have little tilt in the pure DSPE monolayer. Attaching two EO monomers (PEG_{90}) to the DSPE headgroup induces a tilt of the chains, two maxima in the Q_z direction being now evident (Fig. 9). However, the PEG_{90} *lattice* is still predominantly hexagonal, as these two peaks are at almost the same Q_{xy} value (Fig. 8). The ratio of the peak intensities is approximately 1:2 and the positions of their intensity maxima ($Q_z \sim 0$ and $Q_z > 0$) indicate (Als-Nielsen and Kjaer, 1989; Kjaer, 1994) that the molecules tilt approximately towards their nearest neighbor. The packing structure of the lipid monolayer changes further as the number of EO units increases to 8 for PEG_{350}. Again, two maxima in the intensity of the Bragg-rods are evident (Fig. 9), but they occur at two clearly separate Q_{xy}-positions indicating a distortion of the hexagonal cell. The ratio of the

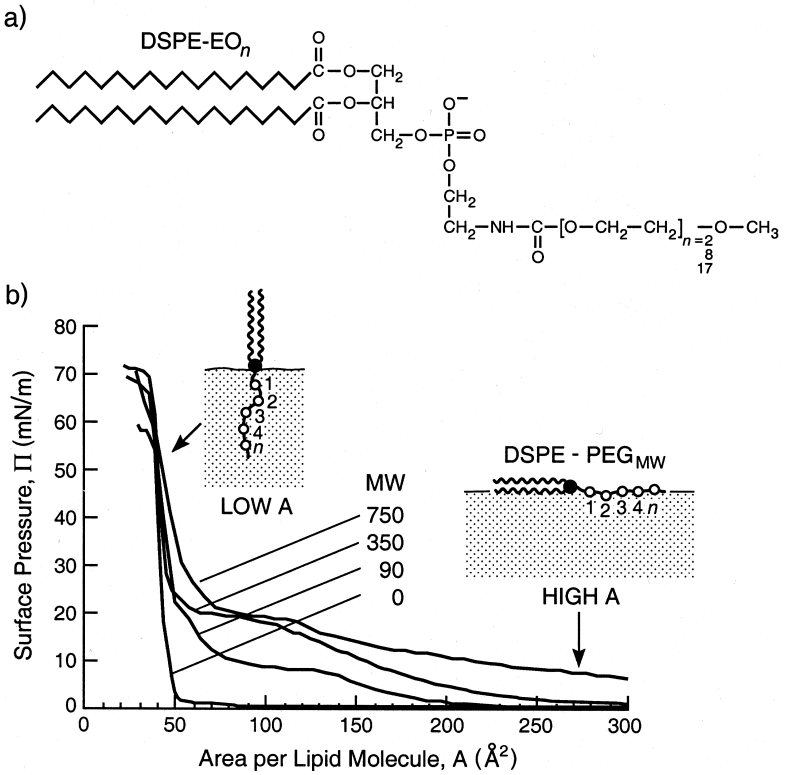

Fig. 7. (a) Model of the PEG–lipid molecule DSPE-EO_n. (b) Monolayer compression (π–A) isotherms of pure DSPE, DSPE-PEG_{90}, DSPE-PEG_{350}, and DSPE-PEG_{750} at 21°C. The area, A, is the mean area per molecule at the air–water interface. At high surface pressures ($\pi > 30$ mN/m) the lateral interactions of the polymer chains are not evident in the pressure isotherm, as the polymer chains are completely submerged in the water subphase. Inset: schematic configuration of DSPE–EO_n at the air–water interface at high and low areas.

intensities and their positions at $Q_z \sim 0$ and $Q_z > 0$ once again indicates that the molecules are tilted towards their nearest neighbors. Upon further increasing the number of EO units to 17, PEG_{750}, the packing within the monolayer changes back to hexagonal (Fig. 8) and only one broad peak at $Q_z \sim 0$ is present, indicating that the molecules are not tilted and stand perpendicular to the interface, Fig. 9.

We find that the in-plane crystallite domain size is 360 Å for pure DSPE and decreases to 58 and 240 Å for PEG_{90}, 63 and 250 Å for PEG_{350}, and a mere 41 Å for PEG_{750}. The out-of-plane coherence length L_c was obtained by fitting the integrated Bragg rod intensities, as shown in Fig. 9. The coherently scattering portion of the lipid tails for unmodified DSPE corresponds to a fully stretched C_{18} chain, $L_c = 23.5$ Å. Similar to the case of the two-component DSPE/DSPE-PEG_{2000} previously discussed system, the coherence length decreases from 23.5 Å to 21.0 and 15.6 Å as the number of EO monomers in the headgroup increases from 0 to 2 and 8. Similarly, the unit cell becomes more distorted from hexagonal packing

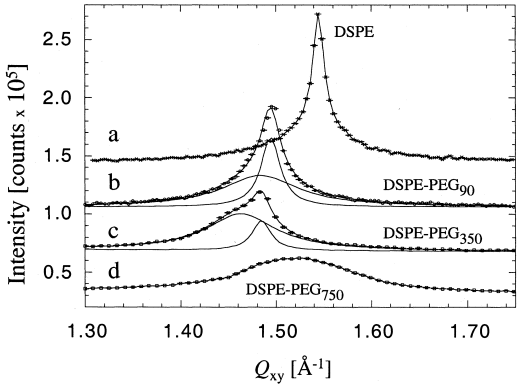

Fig. 8. Grazing-incidence X-ray diffraction data at a surface pressure of 42 mN/m for: (a) pure DSPE; (b) DSPE-PEG_{90}; (c) DSPE-PEG_{350}; (d) DSPE-PEG_{750}. The Bragg peaks profiles were obtained by scanning along the horizontal scattering vector $Q_{xy} = \frac{4\pi \sin \theta_{xy}}{\lambda}$, where $2\theta_{xy}$ is the horizontal angle between the incident and diffracted beam and λ is the wavelength of the X-ray beam and integrating over the whole Q_z-window of the position sensitive detector. For the DSPE-PEG_{90} and DSPE-PEG_{350} monolayers, the Bragg peaks are not symmetric, indicating a small distortion of the hexagonal lattice. These peaks (solid lines) were deconvoluted into two Bragg reflections using a least square fitting procedure.

with little tilt for DSPE to tilted in a slightly distorted lattice for PEG_{90} and to tilted molecules in a more distorted lattice for PEG_{350}, respectively. However, this trend of increasing distortion of the unit cell does not continue. At 17 EO units PEG_{750}, no further reduction in the out-of-plane coherence length occurs, $L_c = 16.0$ Å. Moreover, the in-plane diffraction indicates that the structure returns to hexagonal packing and the molecules once again stand almost perpendicular to the air–water interface with a corresponding decrease in the *d*-spacing. In other words, the unit cell and the packing of the molecules almost return to that of unmodified DSPE, but at the expense of a reduced out-of-plane coherence length, L_c (16.0 vs. 23.5 Å) and size of the scattering islands, L (360 vs. 41 Å).

4.2. X-ray and neutron reflectivity study of polymer–lipid monolayers at the air–water interface

In contrast to the GID measurements, X-ray reflectivity provides information on both the two-dimensional crystalline and amorphous parts of the monolayer. The monolayer electron density distribution was approximated by boxes of various lengths and electron densities, which correspond to the structural components of the layer, e.g. hydrocarbon tails, lipid headgroups, and PEG chains. First, a two box model was tried to describe DSPE; one box for the tail region and another for the headgroup. A single Gaussian roughness was used to smear the interfaces and the resulting model reflectivity was compared to the data. The DSPE-PEG_{MW} (DSPE, DSPE–PEG_{90}, PEG_{350}, and PEG_{750}) monolayers were initially modeled with two boxes also, one for the DSPE tail section and another for the DSPE headgroup–PEG polymer chains. Then the complexity of the model was systematically increased by adding additional boxes, until χ^2 was minimized and no longer significantly decreased upon increasing the number of fitting parameters. This procedure ensured that the problem was not over-parameterized. It was found that in the most complicated case, six boxes were needed to obtain a reasonable fit to the entire reflectivity profile. The fits to the reflectivity data did not signifi-

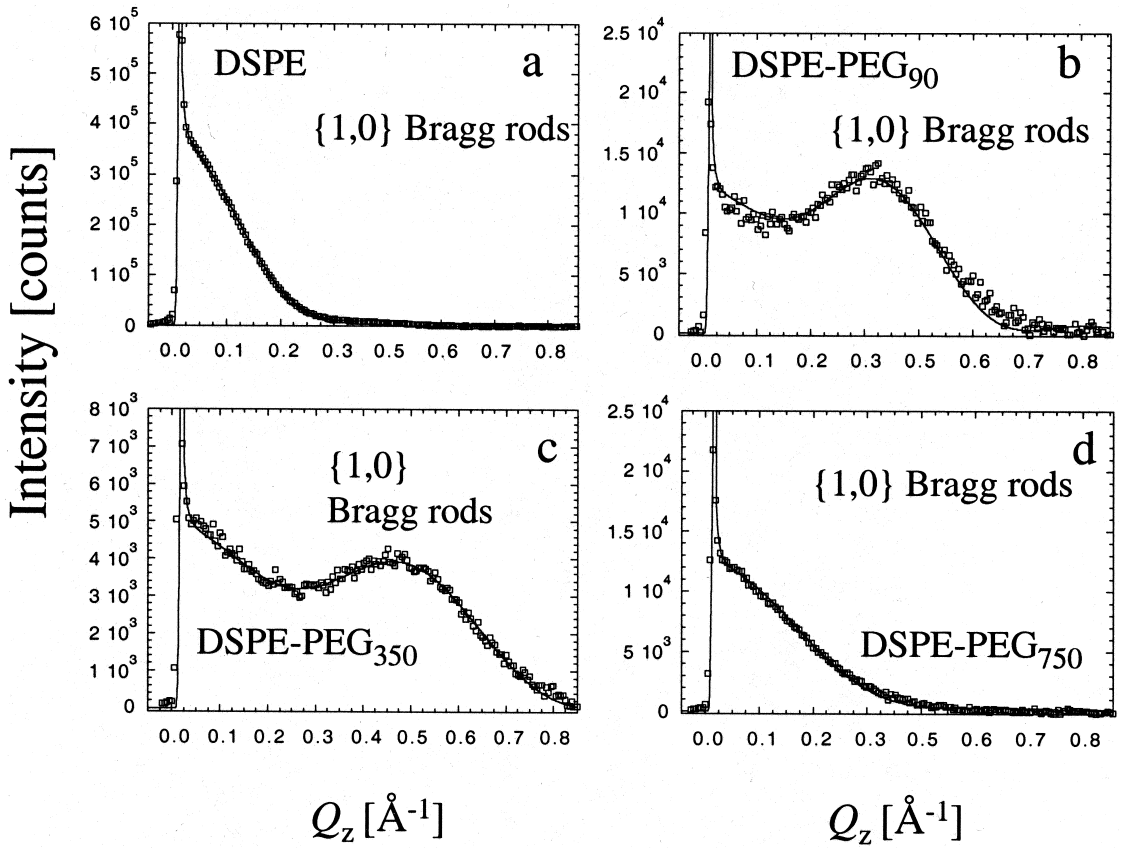

Fig. 9. Bragg rods: scattered intensity distribution perpendicular to the water surface and integrated (after background subtraction) over the Q_{xy} range of each Bragg peak to yield Bragg rods: (a) pure DSPE; (b) DSPE-PEG_{90}; (c) DSPE-PEG_{350}; (d) DSPE-PEG_{750}. The rods were fitted (solid line) by approximating the coherently scattering part of the phospholipid tail by a cylinder of a constant electron density.

cantly improve when an exponential or parabolic form were used to model the polymer layer (Milner et al., 1988; Szleifer and Carignano, 1996) This is most likely due to the short length of the polymer chains used in this study. For this reason, the polymer layer was modeled as a simple step function (Alexander, 1977; de Gennes, 1980).

To obtain a good fit to the DSPE–PEG_{90} reflectivity profiles, a box to account for the polymer layer was added, but it was also found necessary to divide the tail region of the phospholipid into two parts, one with higher electron density located next to the headgroup region and one with lower electron density in contact with air. The total number of electrons within these two boxes was still close to the theoretical electron density of two C_{18} chains. We found it necessary to further divide the headgroup into two boxes as the number of EO monomers increased from 2 to 17 EO units. The fits and electron density profiles obtained from this procedure are shown Fig. 10.

In all cases, the tail region of the lipid layer is 21 ± 0.5 Å thick; however, the electron density distributed between the two boxes composing this layer changes with increasing number of EO units. By modeling the tail region with two boxes, we see that the box representing the tail region adjacent to the lipid headgroups has an electron density slightly greater than that for close packed hydrocarbon chains, while the box against air has a lower than expected electron density. Likewise,

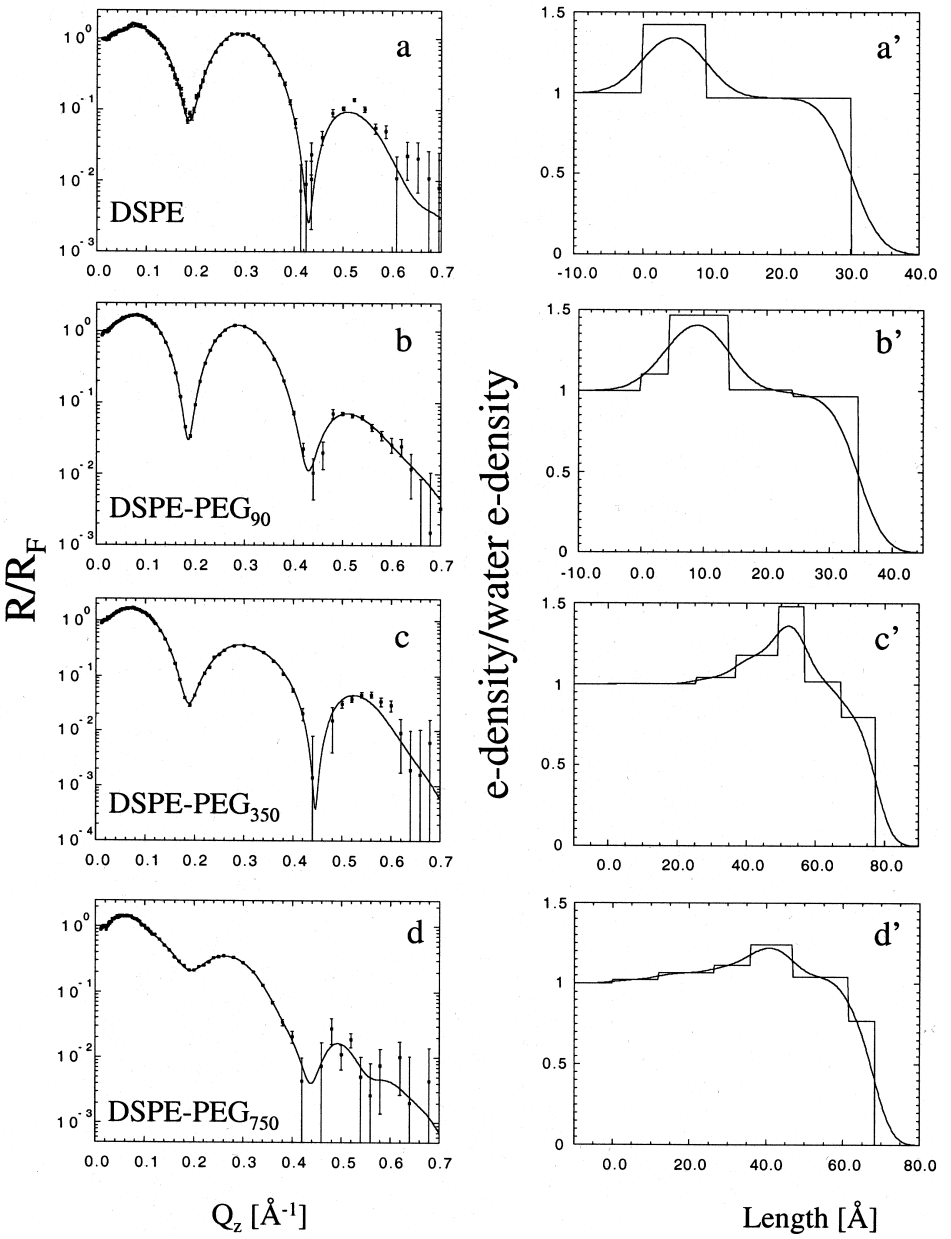

Fig. 10. X-ray reflectivity data at a surface pressure of 42 mN/m for: (a) pure DSPE; (b) DSPE-PEG_{90}; (c) DSPE-PEG_{350}; (d) DSPE-PEG_{750}, the solid lines are fits to the data using box models discussed in the text. (a′, b′, c′, d′) show the corresponding electron density profiles obtained from the fittings. The step-like profiles are the unsmeared electron density profile, while the smooth curves result when the box models are convoluted with the r.m.s. interfacial roughness σ. R/R_F is the measured reflectivity normalized by the Fresnel reflectivity, R_F, for an ideal, infinitely sharp air–water interface.

the boxes used to model the headgroup region have a systematically decreasing electron density (closer to water) but increasing thickness as compared to unmodified DSPE. Indeed, the thickness of the headgroup region doubles from 9 to 20 Å for PEG_{750}. These results imply a mixing and

contribution of different parts of the molecule in each of the boxes, i.e. a mixing of polymer with the lipid headgroup region, headgroup with tail, and participation of air in the tail region. These changes are most likely due to staggering of molecules and structural rearrangements. Finally, the thickness of the polymer layer increases with increasing number of EO units. The weak contrast between PEG and water makes it difficult to quantify the extent and density of this layer. However, as shown in Fig. 10 a region of higher scattering density as compared to water slowly decays from the headgroup region into the water subphase. Finally, there is only a moderate increase in the r.m.s. roughness σ of the monolayer as the number of EO units increases.

We see staggering of the lipid molecules by reflectivity as well as in the GID. Both the tail and headgroup regions must be divided into higher and lower scattering density boxes. A plausible model of this structure is depicted in Fig. 11. By combining the structural data obtained from the GID and reflectivity measurements, we estimate the maximum staggering or lipid–lipid offset to be approximately 10 Å, e.g. the coherence length decreases from 23.5 to 15.6 Å. Likewise, good fits were obtained to the reflectivity data only when the head and tail regions were divided into 10 Å regions of differing electron density. This 10 Å of staggering also corresponds to the size of an unmodified DSPE headgroup. These results taken together with the distortions in the

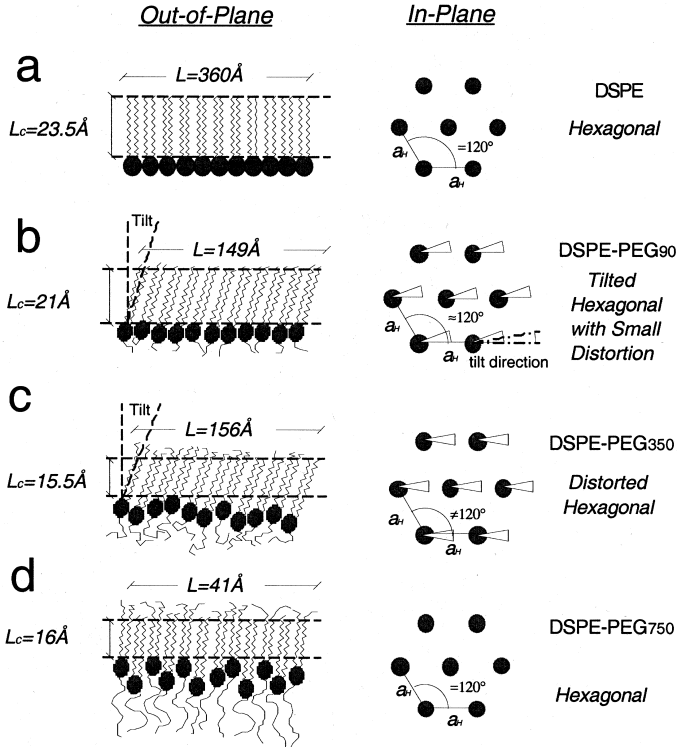

Fig. 11. Schematic of how the out-of-plane and in-plane structure of the lipid monolayers changes with increasing EO monomer units. With increasing number of EO monomers the coherently scattering portion of the lipid tails, L_c, decreases from 23.5, 21.0, 15.6, to 16.0 Å for DSPE, DSPE-PEG_{90}, DSPE-PEG_{350}, and DSPE-PEG_{750}, respectively. Evidently, the tail end (against air), as well as the tail part nearest to the lipid head, become more out of registry and these portions of the hydrocarbon layer become more and more disordered as depicted schematically. As a result, the molecules obtain more space for lateral disorder, but no longer Bragg scatter so the out-of-plane coherence length decreases. Similarly, the unit cell becomes more distorted with increasing PEG MW. However, this trend does not continue as the number of monomers increases from 8 to 17. For chains greater than 14 monomers, it may be possible for PEG to form helices. Interdigitation of neighboring helical chains would be another way of reducing the lateral PEG–PEG repulsion.

unit cell and different packing modes from tilted hexagonal to tilted rectangular and back to non-tilted hexagonal for PEG_{90}, PEG_{350}, and PEG_{750}, respectively, suggest that the lateral PEG modified headgroup–headgroup repulsion was reduced through two different modes. One, by *increasing the area per molecule* and molecular tilt which thereby reduces the headgroup–headgroup interaction. Two, this repulsion was also reduced by *staggering the headgroups* out of the monolayer plane.

It was surprising that the trend of greater unit cell distortion and reduced out-of-plane coherence length L_c, did not continue as the number of EO monomers increased from 2 (PEG_{90}) and 8 (PEG_{350}) to 17 (PEG_{750}). One possible explanation for this behavior is a structural change induced or stabilized by increasing the number of EO monomers (Harder et al., 1998; Pertsin et al., 1998). PEG can form hydrogen bonds both with itself and with water. PEG is known to form helical coils in the solid phase and to retain some of this helical structure in water (Miyazawa, 1961; Miyazawa et al., 1963; Koenig and Angood, 1970; Sandell and Goring, 1971). From X-ray diffraction measurements, the pitch of these helices in the solid phase is 19 Å and composed of 14 EO monomers (Miyazawa, 1961; Koenig and Angood, 1970). Thus, if we have two such helices adjacent to each other as in a PEG_{750} monolayer, another way of reducing the lateral headgroup–headgroup or rather PEG-PEG repulsion would be to offset these helices by half the pitch and so enable some interdigitation. Because half the helix pitch correlates well with the size of a lipid headgroup, it may be that interdigitation opens another pathway by which the lateral tension between adjacent molecules may be reduced and the energy of packing is minimized as shown in Fig 11.

Lastly, in contrast to these studies, our work on *mixed* monolayers of DSPE with longer chained DSPE-PEG_{2000} at concentrations up to 9 mol% indicated that the lateral stresses induced by larger polymeric headgroups did not distort the dimensions of the lipid unit cell. Instead, these monolayers reduced the packing stresses predominately through out-of-plane protrusions, similarly to DSPE-PEG_{750}.

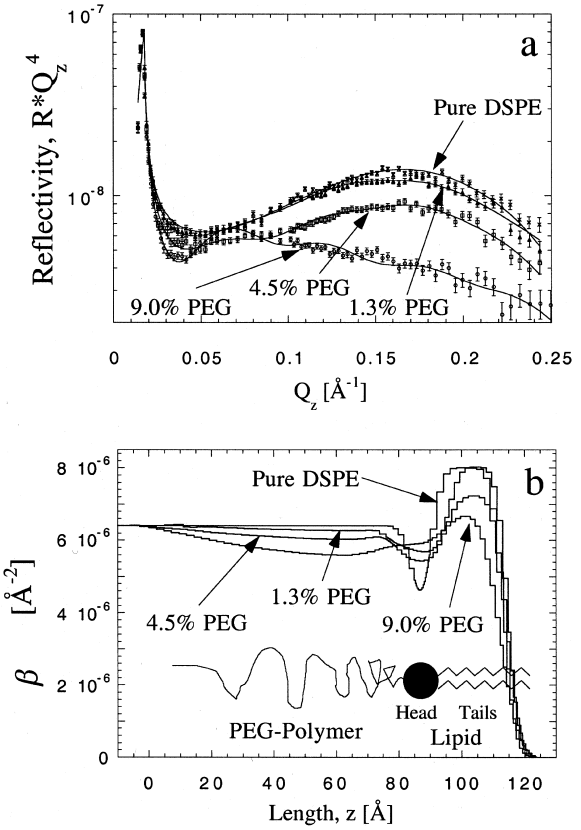

Fig. 12. (a) Neutron reflectivity data for lipid/PEG-lipid monolayers on a pure D_2O subphase. The four reflectivity curves correspond to a pure DSPE monolayer and to mixtures of DSPE and DSPE-EO_{45}. In this set of data, all of the DSPE and DSPE-EO_{45} lipid hydrocarbon chains were fully deuterated. The reflectivity data are plotted as $R \times Q_z^4$ vs. the perpendicular scattering vector Q_z (this accounts for the Q_z^{-4} decrease of the reflectivity due to Fresnel's law). Full lines represent free form fits to the individual measurements and (b) shows scattering length densities $\beta(z)$ obtained from the fits.

In our studies, we could not detect any direct evidence in the GID data of where the PEG portion of the DSPE-PEG molecules is located: no peaks were observed to indicate that the PEG polymer had formed an ordered structure.

In the case of the mixed DSPE/DSPE-PEG_{2000} monolayers, where the electron density difference between the water subphase and the PEG polymer is again very low and therefore difficult to obtain its precise density profile, we measured a series of neutron refelectivities (Majewski et al.,

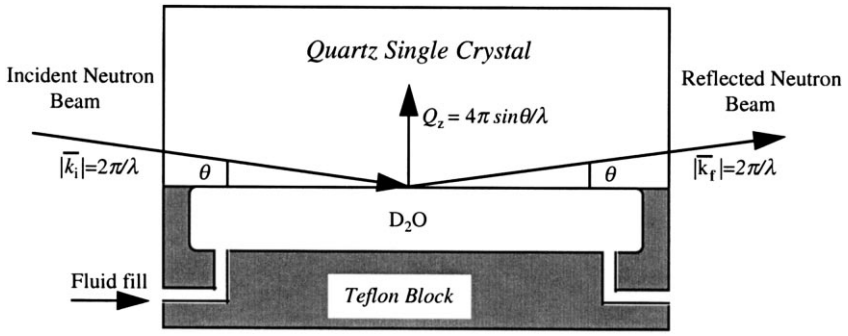

Fig. 13. Diagram of the solid–liquid interface cell used for neutron reflectivity measurements. The neutron beam travels through the solid substrate and is reflected at the solid–solution interface by the organic layers submerged in D_2O. The only contacting surfaces in the cell are quartz or silicon and Teflon.

1997). To increase visiblity of the hydrogenated PEG polymer we used D_2O as the liquid subphase. The polymer SLD was described by a parabolic profile (Milner et al., 1988). The neutron reflectivity data (Fig. 12) showed that the polymer layer thickness increased with PEG–lipid concentration. The average polymer layer thickness changed from 45 to 63 to 70 Å for 1.3 to 4.5

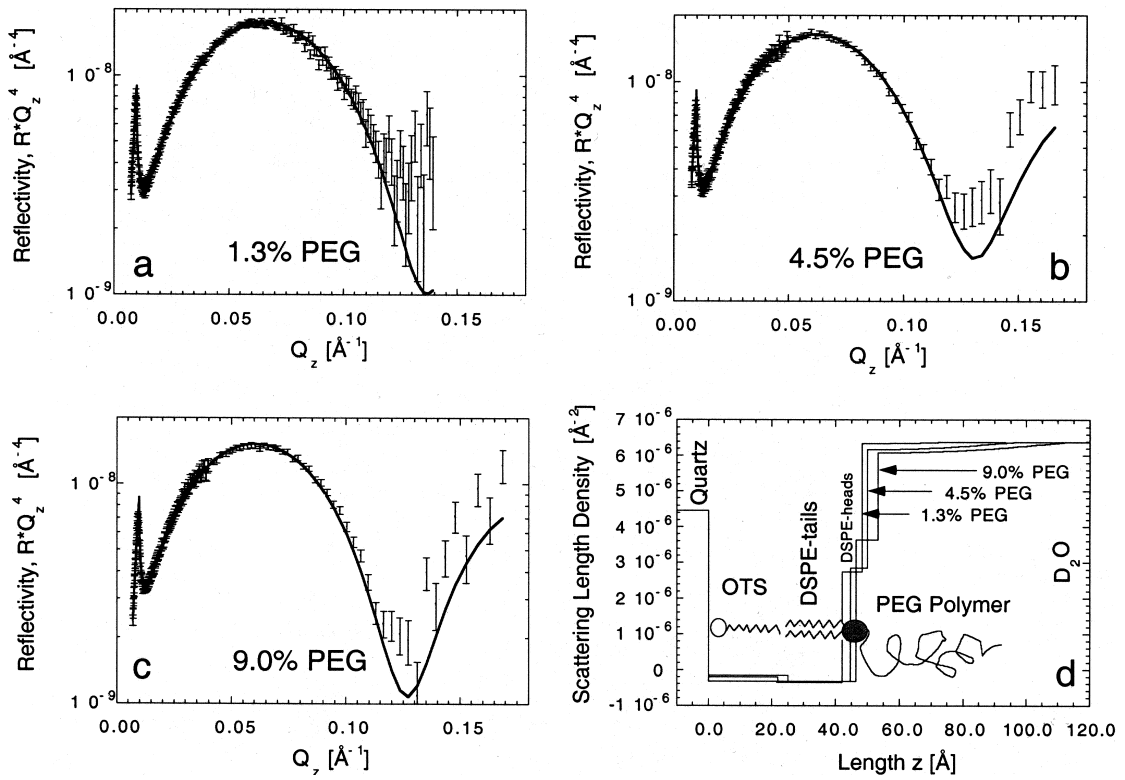

Fig. 14. (a–c) Neutron reflectivity data of the OTS/DSPE/DSPE-PEG_{2000}. The data is well fit by simple boxes for the OTS/DSPE membrane and a parabola for the extended polymer layer. (d) Corresponding scattering length density profile of the model, including the positions of the constituent molecules.

to 9.0%, respectively. This is akin to a mushroom to brush transition in polymers grafted to an interface.

4.3. PEG–lipid monolayers at the solid–liquid interface

Samples were prepared using a solid/liquid cell (Fig. 13) (Baker et al., 1994; Kuhl et al., 1998). Single crystal quartz or silicon blocks were made hydrophobic with a coating of octodecyltrichlorosilane (OTS). A monolayer of PEG–lipids was Langmuir–Blodgett deposited onto the silane-coated surface. The quartz (silicon)-Teflon cell was then assembled under water. The H_2O in the cell was replaced by D_2O for the neutron reflectivity experiments. Because of the penetrating power the neutron can pass though the single crystal and reflect from the solid–liquid interface. Measurements were made for bare substrates, OTS only, 1.3, 4.5 and 9.0% DSPE/DSPE-PEG_{2000} mixtures on each substrate (Kuhl et al., 1998). The bare quartz (silicon) blocks had a roughness of ~ 5 Å. The OTS was characterized first. It was found that on quartz the OTS head and tail lengths were 7.0 ± 1 and 23.7 ± 1 Å, consistent with fully stretched chains and almost 100% surface coverage. On silicon, since the headgroup SLD is very close to silicon oxide, only the tails were discernable. The tail length on silicon was determined to be 19 ± 2 Å which yields an average tilt angle of 34°. The parameters for the OTS were then fixed in the analysis of the lipid data. Fig. 14 shows the neutron reflectivity data and the fitted SLD profiles of OTS/DSPE-PEG bilayers at the quartz–D_2O interface.

In contrast to the air–water interface data, the roughness of the lipid layer did not increase with PEG–lipid concentration. Furthermore, the roughness of the lipid layer was significantly less than that of the substrate. This implies that the OTS has a smoothing effect on the substrate roughness and that out-of-plane fluctuations are suppressed in the lipid by the interaction with the solid surface. Finally, the PEG–polymer thicknesses and densities showed the extension of the polymer into solution as the polymer–polymer interaction increased, consistent with the Langmuir monolayer measurements.

5. Polymer supported lipid assemblies at solid–liquid interfaces

Supported model membranes have been used extensively to study the structure and function of biomembranes (Tamm and McConnell, 1986; Sackmann, 1996). In order for supported membranes to maintain the structural and dynamic properties of free biomembranes, the interaction between the membrane and the substrate should be minimized. Methods to accomplish this include separating the membrane from substrate by either a few monolayers of water, or by soft hydrated polymer or polyelectrolyte film (Sackmann, 1996). The polymer film acts as a support for the biomembrane, not unlike the cytoskeletal support found in actual mammalian cell membranes (Jacobson et al., 1995).

Several strategies can be used for the assembly of biomembranes onto various solid supports and have been recently reviewed (Bangham et al., 1974; Sackmann, 1996; Steinem et al., 1996; Lingler et al., 1997; Puu and Gustafson, 1997). The two major techniques are direct vesicle fusion (Horn, 1984; Bayerl and Bloom, 1990) and the Langmuir–Blodgett technique (Tamm and McConnell, 1986). Furthermore, these two techniques can be combined, i.e. adsorption of vesicles onto pre-formed monolayers as described by various authors (Spinke et al., 1992; Kalb et al., 1992a; Kalb and Tamm, 1992b). While solid-supported membranes have been studied extensively, it is not clear how the presence of a polymer layer affect the assembly process of the biomembrane.

Our work (Wong et al., 1999) focused on the formation of a dimyristoylphophatidylcholine (DMPC) lipid bilayer physisorbed onto branched polyethyleneimine (PEI), a water-soluble polymer which is weakly positively charged in neutral or acidic aqueous environments. In addition, PEI is highly swollen in aqueous environments and thus acts as a deformable and mobile substrate for the biomembrane.

The neutron reflectivity technique has already been used to probe the structure of solid-supported bilayers (Bayerl et al., 1990; Johnson et al., 1991; Koenig et al., 1996). We will report results of our structural investigations resulting from four different methods of preparing PEI-supported DMPC bilayers (Fig. 15) using neutron reflectivity.

5.1. Method 1: Vesicle fusion on dried polymer

The quartz substrate was immersed in a 100 ppm PEI solution of 0.5 mM KNO_3/H_2O (Milli-Q water, pH ~ 7, 15 min) and allowed to dry for approximately 4 h. The neutron reflectivity curve was then measured against air. In the second step, the PEI-coated quartz was transferred into the solid/liquid cell which was filled with D_2O, and DMPC vesicles were added from an aqueous stock suspension (1 mg/ml) to a final concentration of 0.14 mg/ml DMPC.

5.2. Method 2: Polymer adsorption on bilayers (reverse method)

The solid/liquid cell was filled with a solution of 150 mM KNO_3/D_2O, followed by addition of DMPC vesicles (final concentration, 0.14 mg/ml). After the reflectivity curve of the DMPC vesicles on the bare quartz substrate was measured, PEI

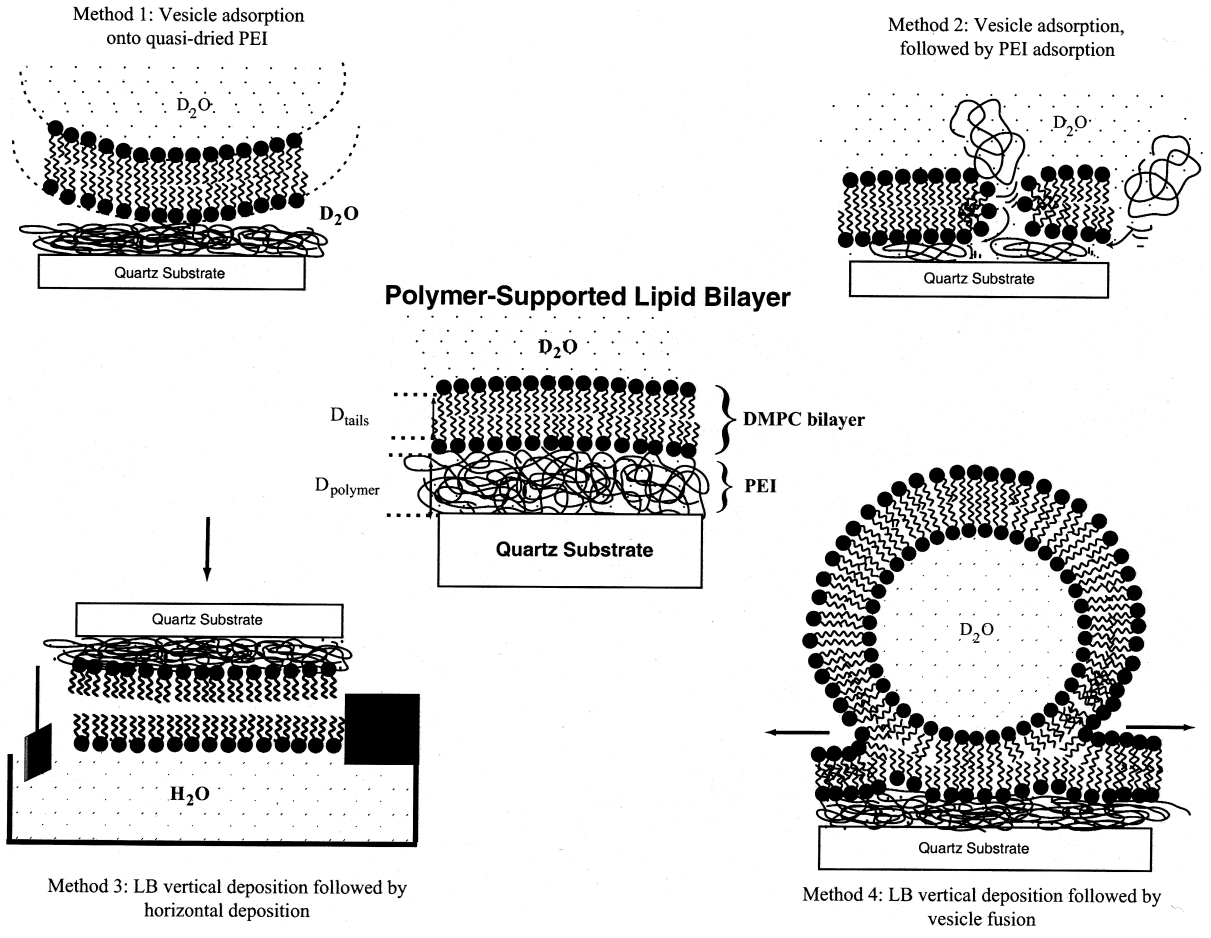

Fig. 15. Schematic of the procedures used to prepare polymer-cushioned bilayers that were then investigated with neutron reflectivity. The methods are labeled as described in the text. Our desired structure is in the center of the diagram.

was added to the system as a 100 ppm solution in 150 mM KNO_3/D_2O.

5.3. Method 3: Langmuir–Blodgett vertical deposition followed by a Langmuir Schaefer horizontal deposition of DMPC monolayers (LB–LS)

A monolayer of hydrogenated DMPC spread at the air–liquid interface of a PEI-containing subphase (100 ppm PEI in 0.5 mM KNO_3/H_2O) was deposited onto the quartz block using the Langmuir–Blodgett method ($\pi = 30 \pm 2$ mN/m). Subsequently, we used the horizontal deposition method to pass the quartz substrate (coated with a PEI-DMPC monolayer) through a monolayer spread onto a pure Millipore water subphase. The solid/liquid interface cell was then assembled under water. The Millipore water was later exchanged by carefully flushing with a 0.5 mM KNO_3/D_2O solution.

5.4. Method 4: Vesicle fusion on polymer supported monolayer ('LB-vesicle fusion')

Again, a monolayer of hydrogenated DMPC spread at the air–liquid interface of a PEI-containing subphase (100 ppm PEI in 0.5 mM KNO_3/H_2O) was deposited onto the quartz substrate using the Langmuir–Blodgett (LB) method as described in the Langmuir–Blodgett/Langmuir–Schaefer method. The DMPC–PEI layer was prepared approximately 15 min prior to measurement of the neutron reflectivity in air. In a second step (after 4 h), the substrate was assembled into the solid/liquid cell and a vesicle solution (final concentration 0.14 mg/ml DMPC) in 0.5 mM KNO_3/D_2O was added.

6. Neutron reflectivity measurements in the liquid–solid interface cell (flow cell)

We used two different geometries to probe the surface of the quartz substrate. When we probed the surface against air, the experiments were performed in an 'upright' geometry, i.e. the quartz on the bottom against air above. When we probed the solid–liquid interface, we used an 'inverted' geometry (Fig. 13), i.e. D_2O on the bottom against quartz above. In both cases the lower medium had a higher scattering length density than the upper one.

6.1. Method 1: Vesicle fusion on dried polymer

The scattering profile of the dried PEI layer on quartz could not be fit with simple one- or two-box models. Satisfactory fits were achieved only with a profile described by a negative step-like scattering length density profile which indicates the presence of H_2O (decreasing in concentration in the direction normal to the surface) within the PEI layer. We found that the PEI layer is significantly hydrated with an average volume ratio of PEI/H_2O approximately 1:3. Thus, the PEI-layer retains a large amount of water and is in a quasi-dried state.

After the addition of a DMPC vesicle-D_2O solution to the *quasi-dried* PEI layer in the solid–liquid interface cell, the resulting reflectivity curve (Fig. 16) can be fit with the SLD profile shown in Fig. 16 (*inset*). The results clearly show the presence of a lipid bilayer on top of a polymer layer, which is in turn, supported by the quartz substrate. From the fitting procedure we found that the total thickness of the PEI layer increases from ~ 110 Å in the quasi-dried state to ~ 180 Å in the hydrated state and ~ 15–20 vol.% polymer is present in the hydrated layer.

From the fit, the thickness of the tails of the DMPC bilayer, is ~ 30 Å. The calculated surface coverage of the DMPC bilayer on the PEI-coated quartz surface is 94%. Therefore, the resulting structure is a fairly complete DMPC bilayer atop a highly hydrated PEI layer.

6.2. Method 2: Polymer adsorption on bilayers (reverse method)

Our neutron scattering studies showed a very complicated neutron reflectivity profile (Fig. 17), when the PEI polymer was injected (and rinsed) into the solid/liquid cell before the DMPC vesicles. From our analysis, we concluded that the structure was comprised of bilayer aggregates

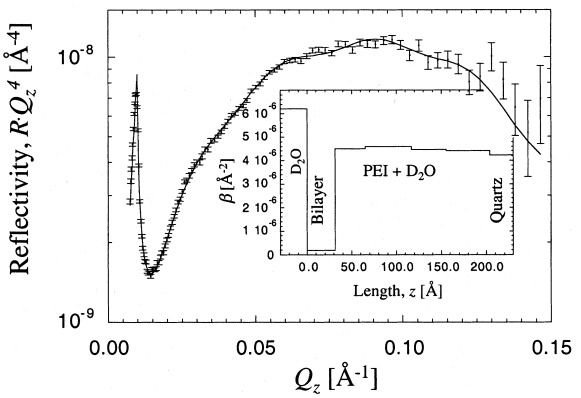

Fig. 16. Neutron reflectivity data of the dried polymer layer after exposure to the DMPC vesicle solution in the flow cell (vesicle fusion on dry polymer method); measurement against D_2O. Insets show the fitted scattering length density profiles.

and/or unfused vesicles with a characteristic length scale of approximately 600 Å. Clearly, the presence of the PEI layer strongly influences the DMPC vesicles' adsorption behavior and fusion into other structures.

However, we found that if there was *no polymer present*, i.e. addition of DMPC vesicles onto a *bare* quartz substrate, this scenario led to an almost perfect bilayer, as previously observed (Johnson et al., 1991; Majewski et al., 1998b). Fig. 18a shows the scattering profile of the DMPC bilayer formed directly on the quartz substrate. The fit using the simple one box model (Fig. 18b) is quite good and gives a value of 36 Å for the lipid tails. The use of a more complicated three-box model to account for the lipid headgroups did not significantly increase the quality of the fit or the value of χ^2. From these fitted densities we find that the lipid membrane in the high salt concentration (150 mM KNO_3) occupies almost 98% of the surface (an almost perfect bilayer) compared to 85% in the low salt case (0.5 mM KNO_3).

After adding PEI to the system, we observed a significant change in the neutron reflectivity curve (Fig. 18a). Our fit shows that the observed change can be attributed to a swollen polymer (PEI/D_2O) layer between DMPC bilayer and the quartz substrate. There is no change in the thickness of the lipid tails and only a moderate increase in their scattering length density. We find that the volume fraction of D_2O in the PEI layer in high salt (83%) agrees with that measured for the low salt conditions (79%). In the high salt case, the overall roughness increased only slightly as compared with the DMPC bilayer on bare quartz, but we observed a change in the scattering length density of the lipid tails. This indicates that the high packing density of the hydrocarbon chains of the bilayer (98%) was partly reduced (91%) by the addition of the PEI resulting in a significant amount of penetration of D_2O or PEI-D_2O into the bilayer region. Such a perturbation of the DMPC bilayer by the PEI layer was not observed in the low salt case.

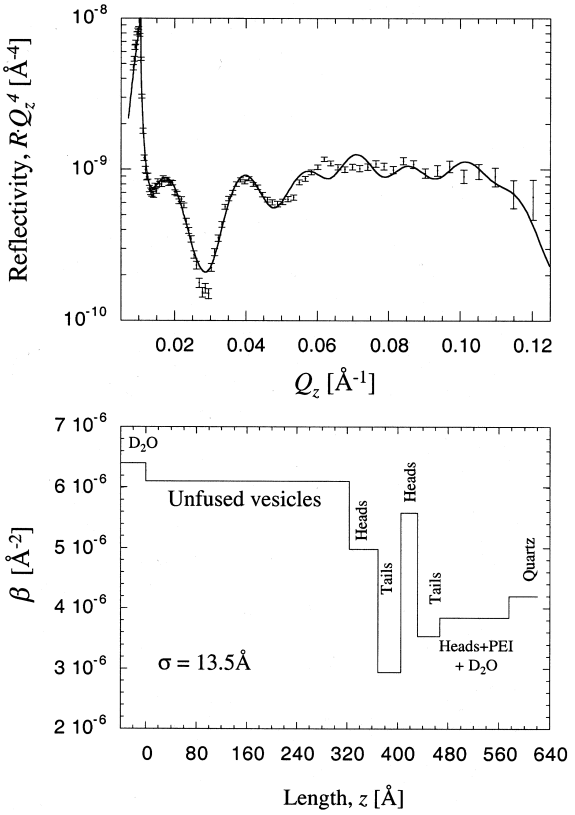

Fig. 17. (a) Neutron reflectivity data at the D_2O-solution interface of PEI adsorbed to a quartz substrate followed by the addition of vesicles. The solid curve through the data is the fit using a multiple box model. (b) Corresponding scattering length density profile of the multiple box model.

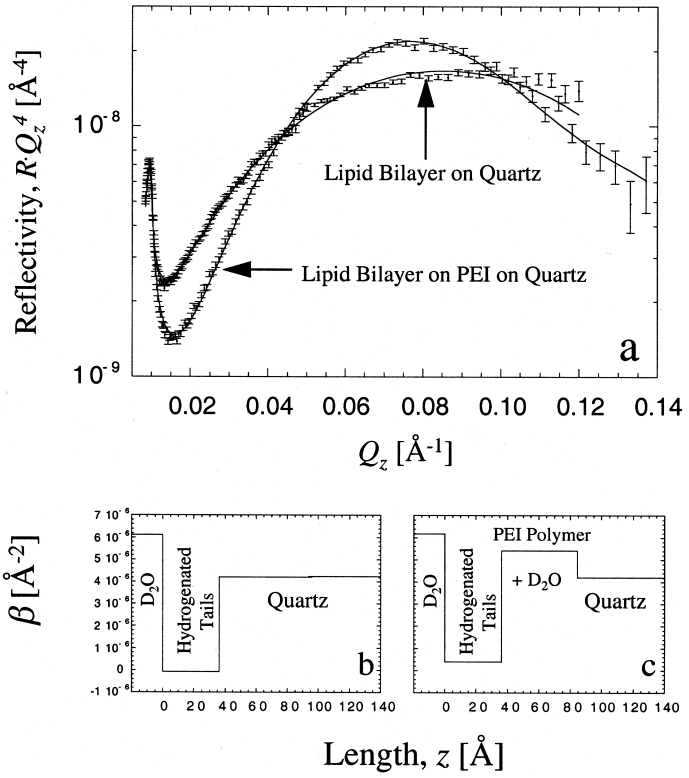

Fig. 18. Neutron reflectivity data of a DMPC bilayer on a bare quartz substrate, followed by PEI adsorption (high salt, 150 mM KNO_3). The bottom part of the Figure shows the corresponding scattering length density profiles.

In order to test the structural stability of the polymer-supported bilayer under high salt conditions, we rinsed the system with 150 mM salt solution. We found that the rinsing had no effect on the membrane.

These results confirm that the reverse preparation procedure gives our desired structure under both low salt (0.5 mM KNO_3) and high salt (150 mM KNO_3) conditions and that the polymer must be able to crawl underneath the formed bilayer, probably via defects in its structure.

6.3. Method 3: Langmuir–Blodgett vertical deposition followed by a Langmuir–Schaefer horizontal deposition of DMPC monolayers (LB–LS)

We used the Langmuir–Blodgett vertical dipping method to deposit a PEI-supported mono-

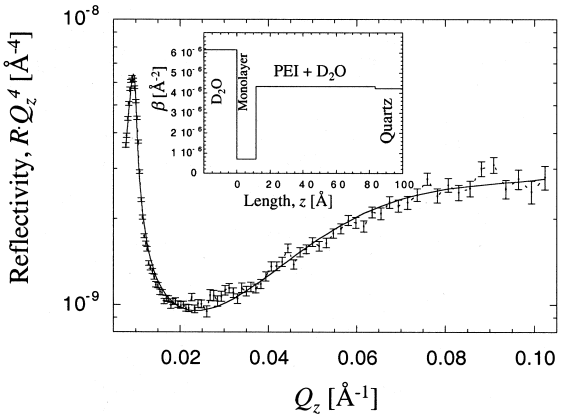

Fig. 19. Neutron reflectivity curves obtained after applying the horizontal dipping procedure (LB–LS method) to prepare polymer-cushioned bilayers. Inset shows the fitted scattering length density profile β. The obtained thickness, 11 Å, suggests the presence of a single monolayer of hydrogenated DMPC.

layer of hydrogenated DMPC onto a quartz substrate. After the formation of the first monolayer which was later confirmed by neutron scattering we attempted to add a second DMPC monolayer using the Langmuir–Schaefer horizontal dipping method. Fig. 19 shows the scattering profile and the resulting structure. From the fit, the thickness of the box representing the DMPC lipid tails region was ~11 Å indicating that the horizontal dipping method did not give our desired polymer-supported bilayer structure.

6.4. Method 4: Vesicle fusion on polymer supported monolayer ('LB-vesicle fusion')

Again, we used the Langmuir–Blodgett vertical dipping method to deposit a PEI-supported monolayer of hydrogenated DMPC onto a quartz substrate. Before adding the vesicle solution, we first characterized the PEI supported DMPC monolayer by measuring the neutron reflectivity spectrum in air. The structure could be fit with a two-box model; one box ~24-Å thick for the DMPC monolayer and one 43-Å thick box for the PEI–H_2O layer. After exposure to a vesicle solution in the solid/liquid interface cell, the resulting reflectivity curve (Fig. 20) indicates that a ~34-Å thick, hydrogenated layer was formed on the polymer support. We found that the simplest model which could satisfactorily fit the reflectivity curve had four boxes: one box for the lipid tails and three in series to approximate the scattering length density profile of the aqueous PEI-layer. The calculated surface coverage of the bilayer was approximately 90%. Moreover, the PEI layer appears to undergo swelling, increasing its thickness three-fold from its quasi-dry state (50% vol. PEI, ~45 Å) to its final hydrated state (~15–20% vol. PEI, ~145 Å) upon exposure to the vesicle solution. In short, vesicle adsorption on polymer-supported lipid monolayers also allows the formation of fairly complete DMPC bilayers atop a highly hydrated polymer layer.

We have demonstrated that the neutron reflectivity is a powerful tool to study the architectures of adsorbed small unilamellar lipid vesicles directly onto a polymer-covered quartz substrate to prepare softly-supported biomembranes. As the

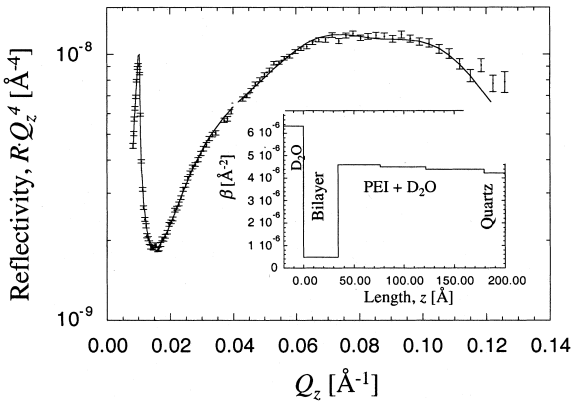

Fig. 20. Neutron reflectivity data illustrating vesicle fusion on monolayer method to prepare a polymer-cushioned bilayer; measurement against D_2O. Inset shows the corresponding scattering length density profile.

results from the vesicle fusion on dry polymer method indicate, the initial drying of the PEI layer before the addition of DMPC vesicles appears to be a critical step needed to form a polymer-cushioned bilayer. This important finding, is in contrast to the situation when we *did not* allow the polymer to dry which resulted in a complex structure consisting mainly of bilayer aggregates and/or unfused vesicles. Moreover, the successful realization of polymer-cushioned lipid bilayers by this simple procedure promises the straightforward incorporation of transmembrane proteins into softly-supported lipid bilayers.

In addition, we confirmed that a reverse procedure in which bilayers are formed on a quartz substrate first and subsequently treated with PEI solution can also be used to form polymer-supported lipid bilayers, under both low (0.5 mM) and high (150 mM KNO_3) salt conditions.

The success of this method shows the importance of balancing the interaction forces between the various components of these assemblies. In our case, there appears to be a strong interaction between the positively-charged PEI layer and the negatively-charged quartz substrate. This electrostatically driven attraction serves to displace the lipids with polymer. Presumably this displacement is aided through defects and flaws in the bilayer.

The situation where the bilayer–substrate attraction dominates the polymer-substrate interaction has been reported. The research group of Sackmann observed that for lipid membranes on dextran, the polymer had to be covalently attached to the underlying substrate in order to prevent the collapse of the lipid–polymer composite film (Elender and Sackmann, 1994; Kühner et al., 1994; Kühner and Sackmann, 1996).

The DMPC-PEI system we have studied is only the first step in an approach of creating model systems for studying with the SFA (Seitz et al., 1998, 1999), AFM and electrophysiological techniques. However, these conditions more closely mimic actual cell membrane environments compared to biomembranes *directly* supported on bare substrates.

7. Conclusions

The scattering techniques used to study monolayers and bilayers yield an array of information crucial to understanding these low dimensional systems. The GID experiments reveal the precise magnitude and direction of chain tilt and the in-plane coherence lengths of the ordered hydrocarbons. The out-of-plane correlations show how molecules stagger, where, in ordered phases, the area/molecule can be determined precisely without the need for modeling. The locations of individual parts of molecules may be located by selective deuteration and a combination of reflection techniques. All of these data, combine to provide insight into the nature of the low dimensional phase transitions observed in thermodynamic measurements such as π-A diagrams. This information sheds light on the complex interactions between amphiphilic molecules. While in this paper we have discussed only the simplest monolayer and bilayer systems, this work has provided a foundation for the study of more complex systems involving proteins and lipids which more closely resemble actual biological systems (see for example Vaknin et al., 1993a,b; Naumann et al., 1994; Thoma et al., 1995, 1996; Brezesinski et al., 1996; Franz et al., 1998).

Acknowledgements

This work was supported under the auspices of the United States Department of Energy. The Manuel Lujan Jr, Neutron Scattering Center is a national user facility funded by the United States Department of Energy, Office of Basic Energy Sciences-Materials Science, under contract number W-7405-ENG-36 with the University of California.

References

Alexander, S., 1977. Adsorption of chain molecules with a polar head. A scaling description. J. Phys. 38, 983–987.

Als-Nielsen, J., Christensen, F., Pershan, P.S., 1982. Smectic-A order at the surface of a nematic liquid crystal: synchrotron X-ray diffraction. Phys. Rev. Lett. 48, 1107–1110.

Als-Nielsen, J., 1984. X-Ray studies of phase transitions on surfaces. Physica B + C 126, 145–148.

Als-Nielsen, J., 1986a. Solid and liquid surfaces studied by synchrotron X-ray diffraction. In: Schommers, W., von Blanckenhagen, P. (Eds.), . The Structure and Dynamics of Surfaces, 2. Springer-Verlag, New York, pp. 181–221.

Als-Nielsen, J., 1986b. Synchrotron X-ray studies of liquid-vapour interfaces. Physica 140A. North-Holland Amsterdam, pp. 376–389.

Als-Nielsen, J., Kjaer, K., 1989. X-ray reflectivity and diffraction studies of liquid surfaces and surfactant monolayers. In: Risteand, T., Sherrington, D., (Eds.), The Proceedings of the NATO Advanced Study Institute, Phase Transitions in Soft Condensed Matter, Geilo, Norway, April 4–April 14, Plenum Publishing, New York, pp. 113–137.

Als-Nielsen, J., Jacquemain, D., Kjaer, K., Lahav, M., Leveiller, F., Leiserowitz, L., 1994. Principles and applications of grazing incidence X-ray and neutron scattering from ordered molecular monolayers at the air–water interface. Phys. Rep. 246, 251–313.

Baker, S.M., Butler, P.D., Hamilton, W.A., Hayter, J.B., Smith, G.S., 1994. Shear cell for the study of liquid–solid interfaces by neutron reflectometry. Rev. Sci. Instr. 65 (2), 412–416.

Bangham, A.D., Hill, M.W., Miller, N.G., 1974. Preparation and use of liposomes as models of biological membranes. Methods Membr. Biol. 1, 1–68.

Bayerl, T.M., Bloom, M., 1990. Physical properties of single phospholipid bilayers adsorbed to micro glass beads — a new vesicular model system studied by H-2-nuclear magnetic resonance. Biophys. J. 58, 357–362.

Bayerl, T.M., Thomas, R.K., Penfold, J., Rennie, A., Sackmann, E., 1990. Specular reflection of neutrons at phospholipid monolayers. Biophys. J. 57, 1095–1098.

Braslau, A., Deutsch, M., Pershan, P.S., Weiss, A.H., Als-Nielsen, J., Bohr, J., 1985. Surface roughness of water measured by X-ray reflectivity. Phys. Rev. Lett. 54, 114–117.

Braslau, A., Pershan, P.S., Swislow, G., Ocko, B.M., Als-Nielsen, J., 1988. Capillary waves on the surface of simple liquids measured by X-ray reflectivity. Phys. Rev. A 38, 2457–2470.

Brezesinski, G., Thoma, M., Struth, B., Möhwald, H., 1996. Structural changes of monolayers at the air/water interface contacted with *n*-alkanes. J. Phys. Chem. 100, 3126–3130.

Eisenberger, P., Marra, W.C., 1981. X-Ray diffraction study of the Ge(001) reconstructed surface. Phys. Rev. Lett. 46, 1081–1084.

Elender, G., Sackmann, E., 1994. Wetting and dewetting of Si/SiO_2-wafers by free and lipid-monolayer covered aqueous solutions under controlled humidity. J. Phys. II 4, 455–479.

Feidenhans'l, R., 1989. Surface structure determination by X-ray diffraction. Surface Science Reports 10. North-Holland, Amsterdam, pp. 105–188.

Franz, H., Dante, S., Wappmannsberger, T.h., Petry, W., de Rosa, M., Rustichelli, F., 1998. An X-ray reflectivity study of monolayers and bilayers of archae lipids on a solid substrate. Thin Solid Films 52/55, 327–329.

de Gennes, P.G., 1980. Conformations of polymer attached to an interface. Macromolecules 13, 1069–1075.

Gunier, A., 1968. X-Ray Diffraction. Freeman, San Francisco.

Halperin, A., 1998. Compression induced phase transition in PEO brushes: the *n*-cluster model. Euro. Phys. J. B 3, 359–364.

Harder, P., Grunze, M., Dahint, R., Whitesides, G.M., Laibinis, P.E., 1998. Molecular conformation in oligo(ethylene glycol)-terminated self-assembled monolayers on gold and silver surfaces determines their ability to resist protein adsorption. J. Phys. Chem. B 102, 426–436.

Helm, C.A., Möhwald, H., Kjaer, K., Als-Nielsen, J., 1987a. Phospholipid monolayer density distribution perpendicular to the water surface. A synchrotron X-ray reflectivity study. Europhys. Lett. 4, 697–703.

Helm, C.A., Möhwald, H., Kjaer, K., Als-Nielsen, J., 1987b. Phospholipid monolayers between fluid and solid states. Biophys. J. 52, 381–389.

Helm, C.A., Tippman-Krayer, P., Möhwald, H., Als-Nielsen, J., Kjaer, K., 1991. Phases of phosphatidyl ethanolamine monolayes studied by synchrotron X-ray scattering. Biophys. J. 60, 1456–1476.

Horn, R.G., 1984. Direct measurement of the force between two lipid bilayers and observation of their fusion. Biochim. Biophys. Acta 778, 224–228.

Jacobson, K., Sheets, E.D., Simson, R., 1995. Revisiting the fluid mosaic model of membranes. Science 268, 1441–1442.

Janiak, M.J., Small, D.M., Shipley, G.G., 1976. Nature of the thermal pretransition of synthetic phospholipids: dimyristoyl- and dipalmitoyllecithin. Biochemistry 15, 4575–4580.

Janiak, M.J., Small, D.M., Shipley, G.G., 1979. Temperature and compositional dependence of the structure of hydrated dimyristoyl lecithin. J. Biol. Chem. 254, 6068–6078.

Joannic, R., Auvaray, L., Lasic, D.D., 1997. Monodisperse vesicles stabilized by grafted polymer. Phys. Rev. Lett. 78, 3402–3405.

Johnson, S.J., Bayerl, T.M., McDermott, D.C. et al., 1991. Structure of an adsorbed dimyristoyl-phosphatidylcholine bilayer measured with specular reflection of neutrons. Biophys. J. 59, 289–294.

Kalb, E., Frey, S., Tamm, L.K., 1992a. Formation of supported planar bilayers by fusion of vesicles to supported phospholipid monolayers. Biochim. Biophys. Acta 1103, 307–316.

Kalb, E., Tamm, L., 1992b. Incorporation of cytochrome b_5 into supported phospholipid bilayers by vesicle fusion to supported monolayers. Thin Solid Films 210/211, 763–765.

Kenworthy, A.K., Simon, S.A., McIntosh, T.J., 1995a. Structure and phase behavior of lipid suspensions containing phospholipids with covalently attached poly(ethylene glycol). Biophys. J. 68, 1903–1920.

Kenworthy, A.K., Hristova, K., Needham, D., McIntosh, T.J., 1995b. Range and magnitude of the steric pressure between bilayers containing phospholipids with covalently attached poly(ethylene glycol). Biophys. J. 68, 1921–1936.

Kjaer, K., Als-Nielsen, J., Helm, C.A., Laxhuber, L.A., Möhwald, H., 1987. Ordering in lipid monolayers studied by synchrotron X-ray diffraction and fluorescence microscopy. Phys. Rev. Lett. 58, 2224–2227.

Kjaer, K., 1994. Some simple ideas on X-ray reflection and grazing-incidence diffraction from thin surfactant films. Physica B 198, 100–109.

Koenig, J.L., Angood, A.C., 1970. Raman spectra of poly(ethylene glycols) in solution. J. Polym. Sci. A2 (8), 1787–1796.

Koenig, B.W., Krueger, S., Orts, W.J. et al., 1996. Neutron reflectivity and atomic force microscopy studies of a lipid bilayer in water adsorbed to the surface of a silicon single crystal. Langmuir 12, 1343–1350.

Kuhl, T., Leckband, D., Lasic, D., Israelachvili, J., 1994. Modulation of interaction forces between bilayers exposing short-chained ethylene oxide headgroups. Biophys. J. 66, 1479–1488.

Kuhl, T.L., Majewski, J., Wong, J.Y., Steinberg, S., Leckband, D.E., Israelachvili, J.N., Smith, G.S., 1998. A neutron reflectivity study of polymer modified phospholipid monolayers at solid-solution interface: PEG-lipid on silane modified substrates. Biophys. J. 75 (5), 2352–2362.

Kuhl, T.L., Majewski, J., Howes, P.B. et al., 1999. Packing stress relaxation in polymer–lipid monolayers at the air–water interface: an X-ray grazing incidence diffraction and reflectivity study. J. Am. Chem. Soc. 121 (33), 7682–7688.

Kühner, M., Sackmann, E., 1996. Ultrathin hydrated dextran films grafted on glass-preparation and characterization of structural, viscous, and elastic properties by quantitative microinterferometry. Langmuir 12, 4866–4876.

Kühner, M., Tampe, R., Sackmann, E., 1994. Lipid mono- and bilayer supported on polymer films — composite polymer–lipid films on solid substrates. Biophys. J. 67, 217–226.

Langmuir, I., 1917. The constitution and fundamental properties of solids and liquids II. Liquids. J. Am. Chem. Soc. 39, 1848–1906.

Lasic, D., Martin, F., 1995. Stealth Liposomes. CRC Press, Boca Raton.

Lingler, S., Rubinstein, I., Knoll, W., Offenhausser, A., 1997. Fusion of small unilamellar lipid vesicles to alkanethiol and thiolipid self-assembled monolayers on gold. Langmuir 13, 7085–7091.

Lovesey, S.W., 1986. Theory of Neutron Scattering from Condensed Matter. Oxford University Press, New York.

Majewski, J., Popovitz-Biro, R., Bouwman, W.G. et al., 1995. The structural properties of uncompressed crystalline monolayers of alcohols $C_nH_{2n+1}OH$ on water and their role as ice nucleators. Chem.-A Eur. J. 1, 304–311.

Majewski, J., Kuhl, T.L., Gerstenberg, M.C., Israelachvili, J.N., Smith, G.S., 1997. Structure of phospholipid monolayers containing poly(ethylene glycol) lipids at the air-water interface. J. Phys. Chem. B 101, 3122–3129.

Majewski, J., Kuhl, T.L., Kjaer, K. et al., 1998a. X-Ray synchrotron study of packing and protrusions of polymer–lipid monolayers at the air–water interface. J. Am. Chem. Soc. 120, 1469–1473.

Majewski, J., Wong, J.Y., Park, C.K., Seitz, M., Israelachvili, J.N., Smith, G.S., 1998b. Structural studies of polymer-cushioned lipid bilayers. Biophys. J. 75, 2363–2367.

Milner, S., Witten, T., Cates, M., 1988. Theory of the grafted polymer brush. Macromolecules 21, 2610–2619.

Miyazawa, T., 1961. Molecular vibrations and structure of high polymers. II. Helical parameters of infinite polymer chains as function of bond lengths, bond angles and internal rotation angles. J. Polym. Sci. 55, 215–230.

Miyazawa, T., Fukushima, K., Ideguchi, Y., 1963. Molecular vibrations and structure of high polymers. III. Polarized infrared spectra, normal vibrations, and helical conformation of polyethylene glycol. J. Chem. Phys. 37, 2764–2776.

Naumann, C., Dietrich, C., Lu, J.R. et al., 1994. Structure of mixed monolayers of dipalmitoyl-glycero-phosphocholine and polyethylene glycol monodecyl ether at the air/water interface determined by neutron reflection and film balance techniques. Langmuir 10, 1919–1925.

Nevot, L., Croce, P., 1980. Characterisation of surfaces by grazing X-ray reflection. Rev. Phys. Appl. 15, 761–779.

Pertsin, A.J., Grunze, M., Garbuzova, I.A., 1998. Low energy configurations of methoxy triethylene glycol terminated alkanethiol self-assembled monolayers and their relevance to protein adsorption. J. Phys. Chem. B 102, 4918–4926.

Puu, G., Gustafson, I., 1997. Planar lipid bilayers on solid supports from liposomes — factors of importance for kinetics and stability. Biochim. Biophys. Acta 1327, 149–161.

Russell, T.P., 1990. X-Ray and neutron reflectivity for the investigation of polymers. Mat. Sci. Rep. 5 (4&5), 171–271.

Sandell, L.S., Goring, D.A.I., 1971. Correlation between the temperature dependence of apparent specific volume and the conformation of oligomeric propylene glycols in aqueous solution. J. Polym. Sci A2 (9), 115–126.

Sackmann, E., 1996. Supported membranes: scientific and practical applications. Science 271, 43–48.

Seitz, M., Park, C.K., Wong, J.Y., Israelachvili, J.N., 1999. Study of the fusion process between solid and soft supported phospholipid bilayers with the surface forces apparatus. In: Warr, G., Manne, S., (Eds.), ACS Symposium Series: Supramolecular Structure in Confined Geometries. ACS, Washington D.C.

Seitz, M., Wong, J.Y., Park, C.K., Alcantar, N.A., Israelachvili, J., 1998. Formation of tethered supported bilayers via membrane-inserting reactive lipids. Thin Solid Films 327/329, 767–771.

Sheth, S.R., Leckband, D., 1997. Measurements of attractive forces between proteins and end-grafted poly(ethylene glycol) chains. Proc. Natl. Acad. Sci. USA 94, 8399–8404.

Spinke, J., Yang, J., Wolf, H., Liley, M., Ringsdorf, H., Knoll, W., 1992. Polymer-supported bilayer on a solid substrate. Biophys. J. 63, 1667–1671.

Smith, G.S., Sirota, E.B., Safinya, C.R., Clark, N.A., 1988. Structure of the L_β phases in a hydrated phosphatidylcholine multimembrane. Phys. Rev. Lett. 60, 813–816.

Smith, G.S., Sirota, E.B., Safinya, C.R., Plano, R.J., Clark, N.A., 1990. X-Ray structural studies of freely suspended ordered hydrated DMPC multimembrane films. J. Chem. Phys. 92, 4519–4529.

Smith, G.S., Majkrzak, C.F., 1999. Neutron reflectometry. In: Prince, E., Wilson, A.J.C. (Eds.), International Tables for Crystallography, Volume C: Mathematical, Physical and Chemical Tables, 2nd Kluwer Academic Publishers, Dordrecht, pp. 126–130.

Steinem, C., Janshoff, A., Ulrich, W.P., Sieber, M., Galla, H.J., 1996. Impedance analysis of supported lipid bilayer membranes — a scrutiny of different preparation techniques. Biochim. Biophys. Acta — Biomembranes 1279, 169–180.

Szleifer, I., Carignano, M.A., 1996. Tethered polymer layers. In: Prigogine, I., Rice, S.A. (Eds.), . Advances in Chemical Physics, 12. John Wiley and Sons, New York, pp. 165–259.

Tamm, L.K., McConnell, H.M., 1986. Supported phospholipid bilayers. Biophys. J. 47, 105–113.

Tirosh, O., Barenholz, Y., Katzhendler, J., Priev, A., 1998. Hydration of polyethylene glycol-grafted liposomes. Biophys. J. 74, 1371–1379.

Thoma, M., Pfohl, T., Möhwald, H., 1995. Thermodynamic relation of an insoluble monolayer at the oil/water interface and at the air/water interface in contact with oil. Langmuir 11, 2881–2888.

Thoma, M., Schwendler, M., Baltes, H. et al., 1996. Ellipsometry and X-ray reflectivity studies on monolayers of phosphatidylethanolamine and phosphatidylcholine in contact with *n*-dodecane, *n*-hexadecane, and bicyclohexyl. Langmuir 12, 1722–1728.

Vaknin, D., Kjaer, K., Als-Nielsen, J., Losche, M., 1991. Structural properties of phosphatidylcholine in a monolayer at the air/water interface. Biophys. J. 59, 1325–1332.

Vaknin, D., Als-Nielsen, J., Piepenstock, M., Lösche, M.,

1993a. Recognition processes at a functionalized lipid surfaces observed with molecular resolution. Biophys. J. 60, 1545–1552.

Vaknin, D., Kjaer, K., Ringsdorf, H. et al., 1993b. X-ray and neutron reflectivity studies of a protein monolayer adsorbed to a functionalized aqueous surface. Langmuir 9, 1171–1174.

Vineyard, G.H., 1982. Grazing-incidence diffraction and the distorted-wave approximation for the study of surfaces. Phys. Rev. B 26, 4146–4159.

Wong, J.Y., Majewski, J., Seitz, M., Park, C.K., Israelachvili, J.N., Smith, G.S., 1999. Polymer-cushioned bilayers. I. A structural study of various preparation methods using neutron reflectometry. Biophys. J. 77, 1445–1457.